Search for Neutral Higgs Boson Production in the Decay $h \to \tau_\mu\tau$ with the DØ Detector

Mark Owen

On Behalf of the DØ Collaboration

School of Physics and Astronomy, University of Manchester, Oxford Road, M13 9PL, UK

A search for the production of neutral Higgs bosons decaying into $\tau^+\tau^-$ final states is presented. One of the two τ leptons is required to decay into a muon. The data were collected by the DØ detector and correspond to an integrated luminosity of about 1.0 fb^{-1}. No excess is observed above the expected backgrounds. The results are interpreted in the Minimal Supersymmetric Standard Model. In the mass range $90 < m_A < 200$ GeV values of $\tan\beta$ larger than 40-60 are excluded for the no-mixing and the m_h^{max} benchmark scenarios.

1 Introduction

The contribution of $\tau^+\tau^-$ final states from the Standard Model (SM) Higgs production is too small to play any role in the SM Higgs searches in p$\overline{\text{p}}$ collision at the Tevatron due to the large irreducible background from $Z \to \tau^+\tau^-$ production. This is different in the Minimal Supersymmetric Standard Model (MSSM), which introduces two Higgs doublets leading to five Higgs bosons: a pair of charged Higgs boson (H$^\pm$); two neutral CP-even Higgs bosons (h,H) and a CP-odd Higgs boson (A). At tree level, the Higgs sector of the MSSM is fully described by two parameters, which are chosen to be the mass of the CP-odd Higgs, m_A, and the ratio of the vacuum expectation values of the two Higgs doublets, $\tan\beta$. The Higgs production cross-section is enhanced in the region of high $\tan\beta$[1]. In the low m_A, high $\tan\beta$ region of the parameter space, Tevatron searches can therefore probe several MSSM benchmark scenarios extending the search

regions covered by LEP [2]. Inclusive searches for $\phi(= H, h, A) \to \tau\tau$ have been performed with integrated luminosities of $L = 350$ pb^{-1} by DØ [3] and $L = 310$ pb^{-1} by CDF [4]. Both searches require at least one τ lepton to decay into an electron (τ_e) or a muon (τ_μ). In this analysis, only the decay $\phi \to \tau_\mu\tau$ is considered using an integrated luminosity of $L = 1.0$ fb^{-1}. CDF has also recently released a preliminary result with $L = 1.0$ fb^{-1} [5]. The biggest improvement in sensitivity compared to the previous analysis comes from using a neural network to improve the separation between signal and background.

2 Event Preselection

The preselection requires one isolated muon with, $p_T^\mu > 15$ GeV. The event is required to have no other muon that is matched to a track in the central detector with $p_T^\mu > 10$ GeV.

Hadronically decaying taus are characterized by a narrow isolated jet that is associated with three or less tracks. Three types of hadronically decaying taus are distinguished:

Type 1: Calorimeter energy cluster, with one associated track and no electromagnetic sub-cluster. This corresponds mainly to the decay $\tau^\pm \to \pi^\pm\nu$.

Type 2: Calorimeter energy cluster, with one associated track and at least one electromagnetic sub-cluster. This corresponds mainly to the decay $\tau^\pm \to \pi^\pm\pi^0\nu$.

Type 3: Calorimeter energy cluster, with three associated tracks, with an invariant mass below 1.7 GeV. This corresponds mainly to the decays $\tau^\pm \to \pi^\pm\pi^\pm\pi^\mp(\pi^0)\nu$.

Tau decays into electrons are usually reconstructed as type-2 taus. These are not removed from the sample. The event is required to contain a τ candidate at a distance $\Delta R > 0.5$ from the muon direction. The charge of the τ candidate must be opposite to the muon charge. The transverse momentum p_T^τ of the τ candidate measured in the calorimeter must be greater than 15 GeV for τ-type 1 and 2, and greater than 20 GeV for τ-type 3. At the same time the transverse momentum of the track associated with the τ candidate is required to be $p_T > 15$ GeV for τ-type 1 and $p_T > 5$ GeV for τ-type 2. In the case of τ-type 3, the scalar sum of the transverse momenta of all associated tracks must be greater than 15 GeV.

3 W $\to \mu\nu$ and Multi-jet Background Estimation

The shape of the W $\to \mu\nu + $ jet background distribution, where the jet is misidentified as a tau, was simulated using PYTHIA. The normalization, however, was obtained using data.

A contribution to the background is expected from heavy flavour multi-jet events, where a muon from a semi-leptonic decay passes the isolation requirement and a jet is mis-identified as a τ candidate. In addition, a contribution is expected from light quark multi-jet events where the jets fake both the tau and the muon. The multi-jet background shape is taken from events with at least one muon and one τ candidate where the muon failed the calorimeter isolation requirement. The normalization of this semi-isolated sample was obtained in a multi-jet enriched sample.

4 Final Event Selection

A set of neural networks, one for each tau type, has been developed to separate the tau leptons from jets. These neural networks make use of input variables that exploit the tau signature such as longitudinal and transverse shower shapes and isolation in the calorimeter and the tracker. The neural network is trained using tau MC events as signal and multi-jet events from data as background to produce a variable that peaks near one for real taus and zero for jets. The tau

candidate is required to have a neural network output greater than 0.9. In the case of type-3 taus this is tightened to 0.95 due to the larger multi-jet background.

It is also possible for muons to fake type-1 or type-2 tau candidates. These fakes are removed by ensuring that type-1 or type-2 tau candidates do not match to a reconstructed muon within a cone of radius $\Delta R_{\mu\tau} = 0.5$.

After selecting events with a high neural network output, there is still a considerable amount of background from W + jets production. To remove these events, the reconstructed W boson mass, $M_{\mathrm{W}} = \sqrt{2E^\nu E^\mu(1 - \cos\Delta\phi)}$ is used, where $E^\nu = \not{E}_{\mathrm{T}} p^\mu / p_{\mathrm{T}}^\mu$ is the estimated neutrino energy, calculated using the ratio of the muon momentum p^μ and muon transverse momentum p_{T}^μ. For real W boson decays, this variable peaks near the W boson mass, whereas for the signal and the Z $\to \tau\tau$ background the variable peaks at zero. Events with $M_{\mathrm{W}} > 20$ GeV are rejected.

To achieve the best separation of the signal from background, neural networks were trained for different Higgs mass points using kinematical variables. The distribution of the visible mass M_{vis} and the optimised neural networks for a Higgs mass of 160 GeV is shown in Figure 1. There is good agreement between the background expectation and the data.
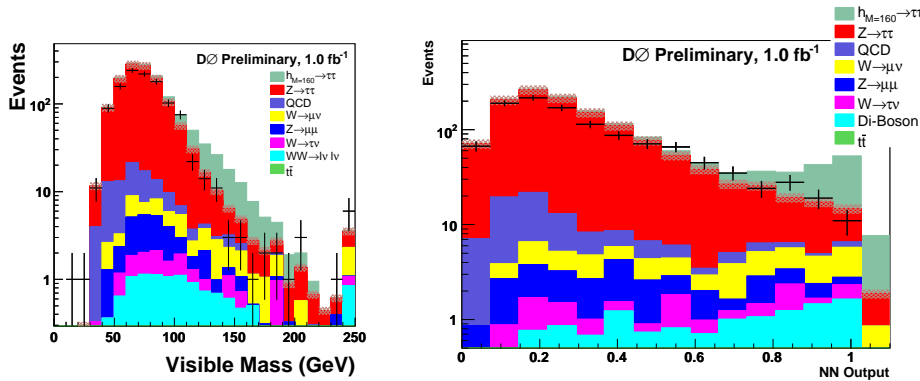

Figure 1: Distribution of a) the visible mass M_{vis} and b) neural network output distribution for a Higgs mass of 160 GeV with all selections applied. The data, shown with error bars, are compared to the sum of the expected backgrounds. Overflow events are added to the last bin. Also shown, in light green, is the signal for a Higgs mass of 160 GeV, normalized to a cross-section of 10 pb. The systematic uncertainty on the background normalisation is 10% and is shown by the shaded area.

5 Results and Conclusion

Limits on the cross-section for Higgs boson production times the branching fraction into tau leptons are derived at 95% Confidence Level (CL). The output from the neural networks, shown in Figure 1 for one mass point, are used in the limit calculation. The distributions for the three tau types are used separately. The cross-section limits are calculated with the CL$_{\mathrm{S}}$ method[6].

There are various sources of systematic uncertainties that affect signal and background. The most important are the uncertainty on the integrated luminosity (6.1%), the trigger efficiency (3%), the tau energy scale ($1 - 11\%$), the uncertainty in the signal acceptance due to choice of parton distribution function ($3.9 - 4.6\%$), the uncertainty of the tau track matching efficiency (4%), the uncertainty on the tau reconstruction efficiency (3%), the theoretical uncertainty on the Z cross-section (5%) and the uncertainty on the modeling of the multi-jet background (3%). All systematic uncertainties are included in the calculation of the expected and observed limits, assuming 100% correlation between signal and background where appropriate. The expected and observed limits are shown in Figure 2 as a function of the hypothetical Higgs mass.

In the MSSM, the masses and couplings of the Higgs bosons depend on $\tan\beta$ and m_A at tree level. Radiative corrections introduce additional dependencies on SUSY parameters. In this

analysis, the m_h^{max} and no-mixing scenarios are studied. The corresponding excluded regions in the $\tan\beta - m_A$ plane are shown in Figure 3. The cross-section at each $\tan\beta - m_A$ point was calculated using FeynHiggs 2.5.1 [7] by adding the $gg \to \phi$ and $b\overline{b} \to \phi$ cross-sections for a given m_A.

In the mass region $90 < m_A < 200$ GeV, $\tan\beta$ values larger than 40-60 are excluded for the no-mixing and the m_h^{max} benchmark scenarios. These results are the most constraining limits from the Higgs to $\tau^+\tau^-$ decay channel to date.
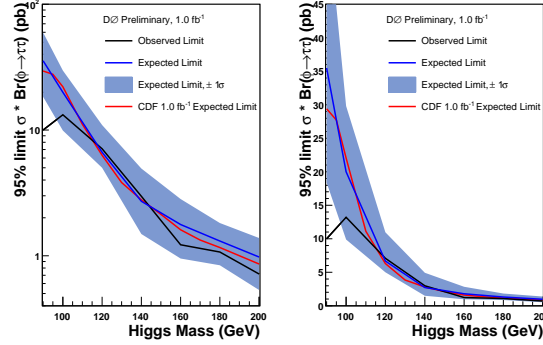

Figure 2: Observed and expected 95% Confidence Level upper limit on the cross-section times branching ratio, using the neural network shown on both a log scale and a linear scale. The band represents the $\pm 1\sigma$ uncertainty on the expected limit. Also shown is the expected limit from the recent CDF result.
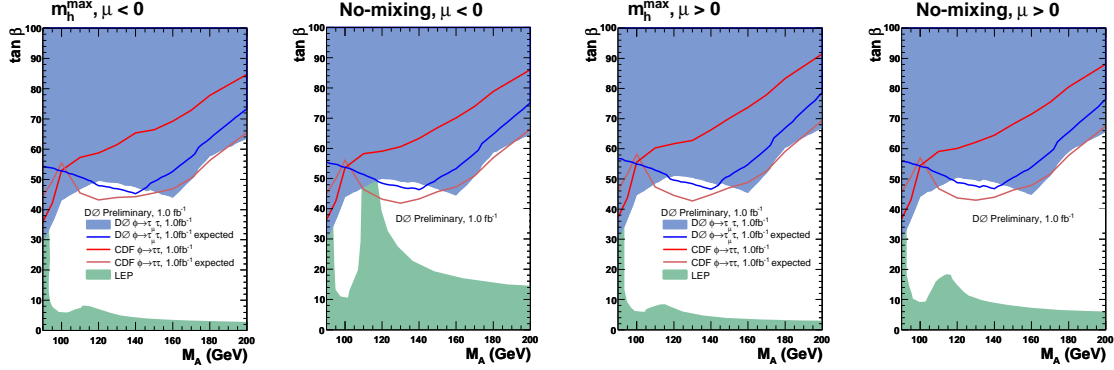

Figure 3: Excluded region in the $\tan\beta - m_A$ plane for $\mu < 0$ in a) the m_h^{max} scenario and b) the no-mixing scenario and excluded region in the $\tan\beta - m_A$ plane for $\mu > 0$ in c) the m_h^{max} scenario and d) the no-mixing scenario.

References

1. M. Carena, S. Heinemeyer, C.E.M Wagner and G. Weiglein, Eur. Phys. J. **C** 45 (2006) 797.
2. The ALEPH, DELPHI, L3 and OPAL Collaborations, LHWG-Note 2005-01.
3. V.M. Abazov *et al.*, Phys. Rev. Lett. **97** (2006) 121802.
4. A. Abulencia *et al.*, Phys. Rev. Lett. **96** (2006) 011802.
5. CDF Collaboration, http://www-cdf.fnal.gov/physics/new/hdg/hdg.html
6. R. Barate *et al.*, Phys. Lett. B **565** (2003) 61; T. Junk, Nucl. Instrum. Meth. A **434** (1999) 435.
7. S. Heinemeyer, W. Hollik, G. Weiglein, Comput. Phys. Commun. **124** (2000) 76.